

3D time-dependent hydrodynamical and radiative transfer modeling of Eta Carinae's innermost fossil colliding wind structures

Thomas Madura¹, T. R. Gull², N. Clementel³, M. Corcoran^{2,4},
A. Damini⁵, K. Hamaguchi^{2,6}, D. J. Hillier⁷, A. F. J. Moffat⁸,
N. Richardson⁹ and G. Weigelt¹⁰

¹San José State University,
One Washington Square, San José, CA 95192-0106, USA
email: thomas.madura@sjsu.edu

²NASA Goddard Space Flight Center, Greenbelt, MD 20771, USA

³Katholieke Universiteit Leuven, Celestijnenlaan 200D, 3001 Leuven, Belgium

⁴The Catholic University of America, Washington, DC 20064, USA

⁵IAG-USP, Rua do Matao 1226, Cidade Universitaria, Sao Paulo 05508-900, Brazil

⁶University of Maryland, Baltimore County, 1000 Hilltop Circle, Baltimore, MD 21250, USA

⁷University of Pittsburgh, 3941 OHara Street, Pittsburgh, PA 15260, USA

⁸Universite de Montreal, CP 6128 Succ. A., Centre-Ville, Montreal, Quebec H3C 3J7, Canada

⁹University of Toledo, Toledo, OH 43606-3390, USA

¹⁰Max-Planck-Institut für Radioastronomie, Auf dem Hügel 69, D-53121 Bonn, Germany

Abstract. Eta Carinae is the most massive active binary within 10,000 light-years. While famous for the largest non-terminal stellar explosion ever recorded, observations reveal a supermassive ($\sim 120 M_{\odot}$) binary consisting of an LBV and either a WR or extreme O star in a very eccentric orbit ($e = 0.9$) with a 5.54-year period. Dramatic changes across multiple wavelengths are routinely observed as the stars move about in their highly elliptical orbits, especially around periastron when the hot (~ 40 kK) companion star delves deep into the denser and much cooler (~ 15 kK) extended wind photosphere of the LBV primary. Many of these changes are due to a dynamic wind-wind collision region (WWCR) that forms between the stars, plus expanding radiation-illuminated fossil WWCRs formed one, two, and three 5.54-year orbital cycles ago. These fossil WWCRs have been spatially and spectrally resolved by the *Hubble Space Telescope*/Space Telescope Imaging Spectrograph (*HST*/STIS) at multiple epochs, resulting in data cubes that spatially map Eta Carinae's innermost WWCRs and follow temporal changes in several forbidden emission lines (e.g. [Fe III] 4659 Å, [Fe II] 4815 Å) across the 5.54-year cycle. We present initial results of 3D time-dependent hydrodynamical and radiative-transfer simulations of the Eta Carinae binary and its WWCRs with the goal of producing synthetic data cubes of forbidden emission lines for comparison to the available *HST*/STIS observations. Comparison of the theoretical models to the observations reveals important details about the binary's orbital motion, photoionization properties, and recent (5 – 15 year) mass loss history. Such an analysis also provides a baseline for following future changes in Eta Carinae, essential for understanding the late-stage evolution of a nearby supernova progenitor. Our modeling methods can also be adapted to a number of other colliding wind binary systems (e.g. WR 140) that are scheduled to be studied with future observatories (e.g. the James Webb Space Telescope).

Keywords. hydrodynamics, radiative transfer, line: formation, methods: numerical, stars: individual (Eta Carinae), stars: mass loss, stars: winds, outflows

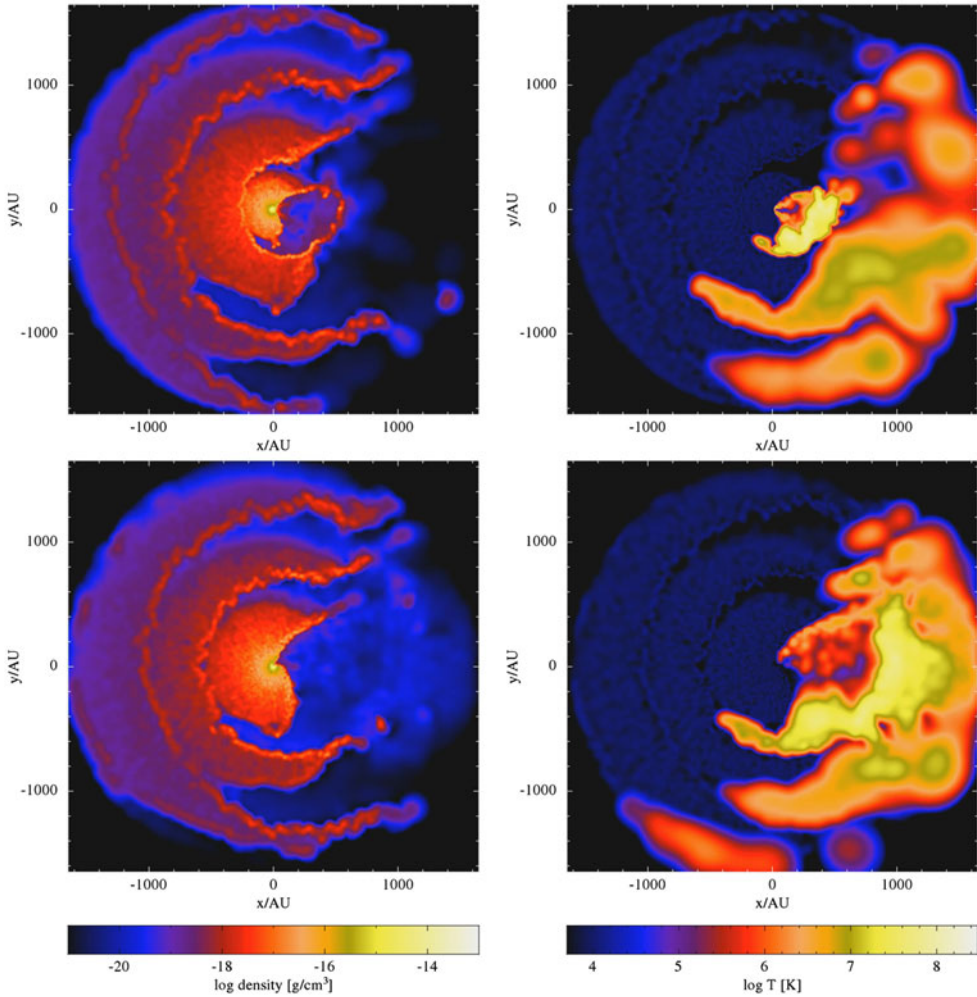


Figure 1. Slices showing log density (left) and log temperature (right) at apastron (top row) and periastron (bottom row) in the orbital xy plane from a 3D SPH simulation of Eta Carinae’s colliding stellar winds, assuming primary and secondary mass loss rates of $8.5 \times 10^{-4} M_{\odot}/\text{yr}$ and $1.4 \times 10^{-5} M_{\odot}/\text{yr}$, and wind terminal speeds of 420 km/s and 3000 km/s, respectively. The orbital semimajor axis length $a = 15.45$ au and the eccentricity $e = 0.9$. The computational domain radius $r \approx 1545$ au $\approx 0.67''$. Axis tick marks correspond to an increment of 155 au.

At 2.3 kpc (Smith 2006), Eta Carinae is the closest and most luminous evolved massive star and supernova progenitor that we can study in great detail, making it an ideal astrophysical laboratory for studying massive binary interactions and stellar wind-wind collisions. Due to their intense luminosities, the stars in Eta Carinae have strong radiation-driven stellar winds. The LBV primary has an incredibly dense wind ($\approx 8.5 \times 10^{-4} M_{\odot}/\text{yr}$, $v_{\infty} \approx 420$ km/s; Hillier *et al.* 2001, Groh *et al.* 2012), while the less luminous companion has a much lower density, but faster wind ($\approx 1.4 \times 10^{-5} M_{\odot}/\text{yr}$, $v_{\infty} \approx 3000$ km/s; Pittard & Corcoran 2002, Parkin *et al.* 2009). These winds violently collide and generate a series of shocks and wind-wind collision regions (WWCRs) that give rise to numerous forms of time-variable emission and absorption seen across a wide range of wavelengths (Damineli *et al.* 2008). Due to the high orbital eccentricity, the

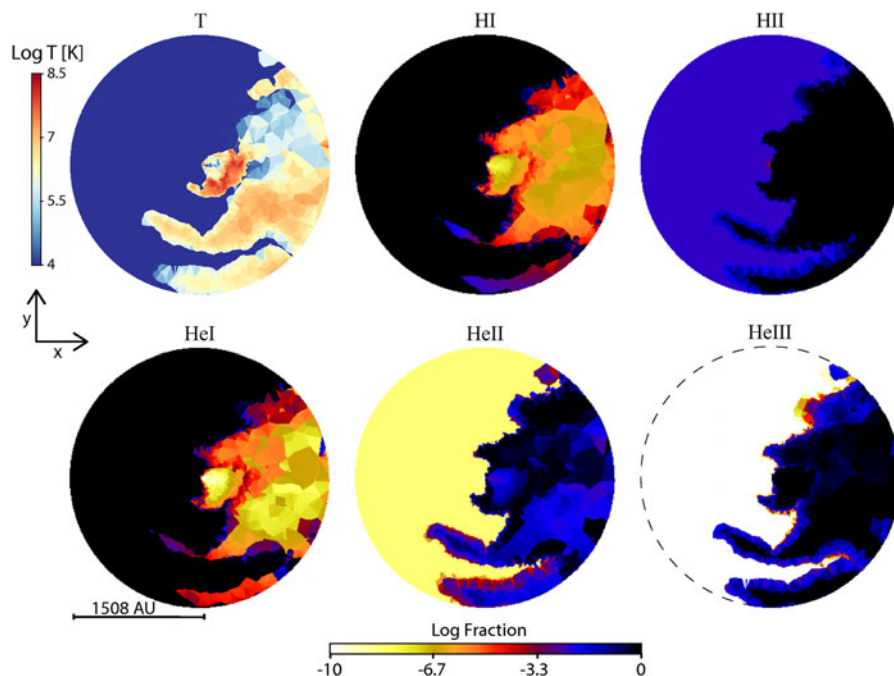


Figure 2. Slices in the orbital plane showing results from a 3D SimpleX radiative transfer simulation of Eta Carinae at apastron. SimpleX was applied to the 3D SPH simulation snapshot shown in the top row of Fig. 1. Color in the above panels shows log temperature (K, top left) and the computed fractions (log scale) of H I (top middle), H II (top right), He I (bottom left), He II (bottom middle), and He III (bottom right).

WWCRs in Eta Carinae produce dense spiral structures of compressed gas irradiated by the hot companion star. These structures have been spatially and spectrally resolved by the *Hubble Space Telescope*/Space Telescope Imaging Spectrograph (*HST*/STIS) in numerous forbidden emission lines (see e.g. Gull *et al.* 2016).

Three-dimensional (3D) Smoothed Particle Hydrodynamics (SPH) simulations have helped to greatly increase our understanding of the Eta Carinae system’s WWCRs and how they affect numerous observational diagnostics (see e.g. Okazaki *et al.* 2008, Madura *et al.* 2012, 2013, Richardson *et al.* 2016). When coupled with 3D radiative transfer simulations, such SPH simulations can be used to obtain detailed 3D maps of ionization fractions of hydrogen, helium, and other elements (Clementel *et al.* 2014, 2015a,b). These model ionization maps help constrain the regions where observed forbidden emission lines can form. From the ionization maps, synthetic data cubes for various forbidden emission lines can be generated and directly compared to available and upcoming *HST*/STIS observations. By comparing the model data cubes to the observations, we hope to place tighter constraints on the binary’s orbital, stellar, wind, and ionization parameters, as well as the system’s recent (5 – 15 year) mass loss history.

Fig. 1 shows density and temperature slices in the orbital plane from a large-scale (computational domain radius $r \approx 1545 \text{ au} \approx 0.67''$) 3D SPH simulation of Eta Carinae’s colliding stellar winds. Visible in the density slices in the left column are the ‘shells’ of compressed primary wind formed after each periastron passage (to the left in the panels) and the extended, open WWCRs that can be illuminated by the companion (to the right in the panels). The temperature panels in the right column of Fig. 1 show the presence of extremely hot ($\gtrsim 10^7 \text{ K}$) gas that is mostly companion star wind material. Such hot gas is responsible for Eta Carinae’s observed X-ray emission.

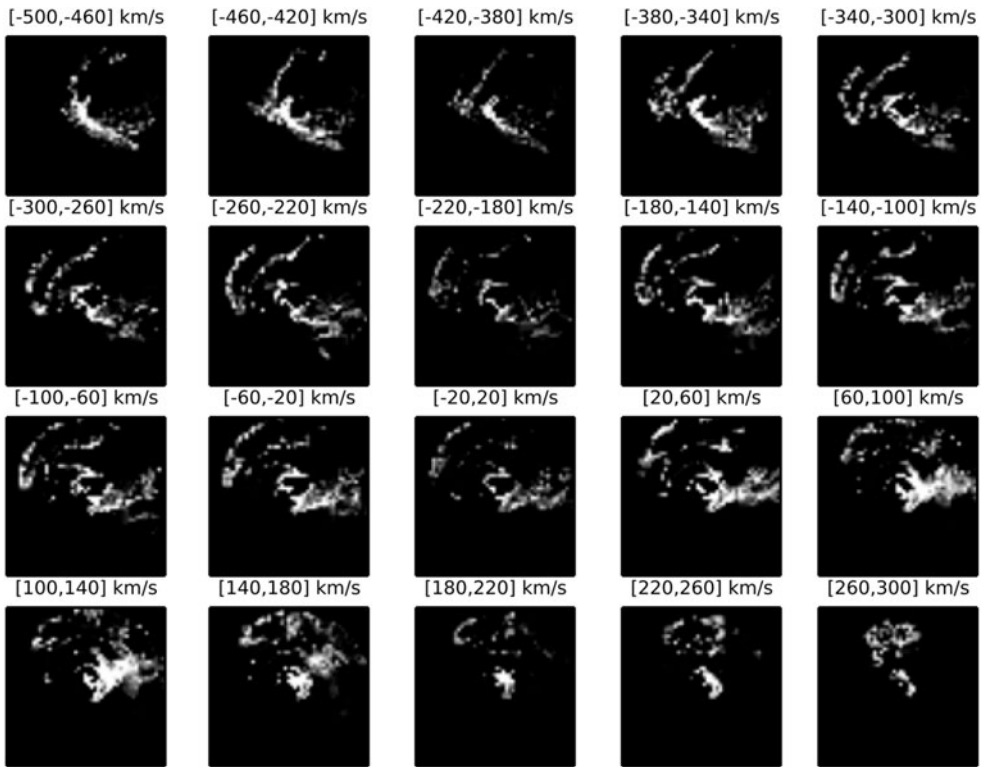


Figure 3. Slices from a synthetic data cube showing the predicted spatial distribution of [Fe III] emission on the sky (North is up) from Eta Carinae’s colliding winds in 40 km/s velocity bins ranging from -500 km/s (upper left) to $+300$ km/s (bottom right). The synthetic [Fe III] emission was computed using the SimpleX results in Fig. 2 and the equations/methods outlined in Madura *et al.* (2012). The width of each panel is $\approx 1.34''$. The color bar is on a square root scale.

Fig. 2 shows the results of applying the SimpleX 3D radiative transfer algorithm to the 3D SPH simulation in Fig. 1 (see Clementel *et al.* 2014, 2015a,b for details on SimpleX and our methods). The equations and methods in Madura *et al.* (2012) can then be applied to the SimpleX results in order to compute synthetic data cubes showing the predicted spatial distribution on the sky of emission from the observed forbidden lines. Example slices from a synthetic data cube of [Fe III] emission are in Fig. 3. Results like those in Fig. 3 can then be compared directly to the observed data cubes presented in e.g. Gull *et al.* (2016) and used to help constrain Eta Carinae’s stellar, wind, and orbital parameters. Work is currently underway to compute synthetic data cubes at multiple orbital phases for direct comparison to the observed [Fe II] and [Fe III] data cubes obtained at multiple epochs and published in Gull *et al.* (2016). Any future observed changes in Eta Carinae’s extended forbidden line emission can also be modeled and used to better understand any changes in the primary LBV’s mass loss rate or the system’s other stellar, wind, or orbital parameters. Other colliding wind binaries (e.g. WR 140) can be similarly modeled.

References

- Clementel, N., Madura, T. I., Kruip, C. J. H., & Paardekooper, J.-P. 2015, *MNRAS*, 450, 1388
 Clementel, N., Madura, T. I., Kruip, C. J. H., Paardekooper, J.-P., & Gull, T. R. 2015, *MNRAS*, 447, 2445

- Clementel, N., Madura, T. I., Kruip, C. J. H., Icke, V., & Gull, T. R. 2014, *MNRAS*, 443, 2475
- Damineli, A., Hillier, D. J., Corcoran, M. F., *et al.* 2008, *MNRAS*, 386, 2330
- Groh, J. H., Hillier, D. J., Madura, T. I., & Weigelt, G. 2012, *MNRAS*, 423, 1623
- Gull, T. R., Madura, T. I., Teodoro, M., *et al.* 2016, *MNRAS*, 462, 3196
- Hillier, D. J., Davidson, K., Ishibashi, K., & Gull, T. 2001, *ApJ*, 553, 837
- Madura, T. I., Gull, T. R., Owocki, S. P., *et al.* 2012, *MNRAS*, 420, 2064
- Madura, T. I., Gull, T. R., Okazaki, A. T., *et al.* 2013, *MNRAS*, 436, 3820
- Okazaki, A. T., Owocki, S. P., Russell, C. M. P., & Corcoran, M. F. 2008, *MNRAS*, 388, L39
- Parkin, E. R., Pittard, J. M., Corcoran, M. F., Hamaguchi, K., & Stevens, I. R. 2009, *MNRAS*, 394, 1758
- Pittard, J. M. & Corcoran, M. F. 2002, *A&A*, 383, 636
- Richardson, N. D., Madura, T. I., St-Jean, L., *et al.* 2016, *MNRAS*, 461, 2540
- Smith, N. 2006, *ApJ*, 644, 1151